

RESEARCH ARTICLE

10.1002/2015WR017703

Key Points:

- Proposed soil hydraulic model includes capillary hysteretic, adsorptive, and film components
- Empirical equations can predict the film conductivity using water retention parameters
- Including vapor conductivity improved conductivity predictions in the very dry range

Supporting Information:

- Data Set S1
- Data Set S2
- Data Set S3
- Data Set S4
- Data Set S5
- Data Set S6
- Data Set S7
- Data Set S8
- Data Set S9
- Data Set S10
- Data Set S11
- Data Set S12
- Data Set S13
- Data Set S14
- Data Set S15
- Data Set S16
- Data Set S17
- Data Set S18

Correspondence to:

Rudiyanto,
lupusae@yahoo.com

Citation:

Rudiyanto, M. Sakai, M. Th. van Genuchten, A. A. Alazba, B. I. Setiawan, and B. Minasny (2015), A complete soil hydraulic model accounting for capillary and adsorptive water retention, capillary and film conductivity, and hysteresis, *Water Resour. Res.*, 51, 8757–8772, doi:10.1002/2015WR017703.

Received 16 JUN 2015

Accepted 14 OCT 2015

Accepted article online 23 OCT 2015

Published online 5 NOV 2015

© 2015. American Geophysical Union.
All Rights Reserved.

A complete soil hydraulic model accounting for capillary and adsorptive water retention, capillary and film conductivity, and hysteresis

Rudiyanto¹, Masaru Sakai², Martinus Th. van Genuchten^{3,4}, A. A. Alazba⁵, Budi Indra Setiawan¹, and Budiman Minasny⁶

¹Department of Civil and Environmental Engineering, Bogor Agricultural University, Bogor, Indonesia, ²Graduate School of Bioresources, Mie University, Tsu, Japan, ³Department of Mechanical Engineering, Federal University of Rio de Janeiro, Rio de Janeiro, Brazil, ⁴Department of Earth Sciences, Utrecht University, Utrecht, Netherlands, ⁵Department of Agricultural Engineering, King Saud University, Riyadh, Saudi Arabia, ⁶Department of Environmental Sciences, The University of Sydney, Sydney, New South Wales, Australia

Abstract A soil hydraulic model that considers capillary hysteretic and adsorptive water retention as well as capillary and film conductivity covering the complete soil moisture range is presented. The model was obtained by incorporating the capillary hysteresis model of Parker and Lenhard into the hydraulic model of Peters-Durner-Iden (PDI) as formulated for the van Genuchten (VG) retention equation. The formulation includes the following processes: capillary hysteresis accounting for air entrapment, closed scanning curves, nonhysteretic sorption of water retention onto mineral surfaces, a hysteretic function for the capillary conductivity, a nonhysteretic function for the film conductivity, and a nearly nonhysteretic function of the conductivity as a function of water content (θ) for the entire range of water contents. The proposed model only requires two additional parameters to describe hysteresis. The model was found to accurately describe observed hysteretic water retention and conductivity data for a dune sand. Using a range of published data sets, relationships could be established between the capillary water retention and film conductivity parameters. Including vapor conductivity improved conductivity descriptions in the very dry range. The resulting model allows predictions of the hydraulic conductivity from saturation until complete dryness using water retention parameters.

1. Introduction

Estimates of the unsaturated soil hydraulic properties are essential for accurate modeling of a range of sub-surface and near-surface hydrological processes, including infiltration, redistribution, evaporation, and solute transport in soils [e.g., *Collis-George*, 2012; *Durner and Flühler*, 2005; *Saito et al.*, 2006; *Šimůnek*, 2005]. The soil hydraulic (constitutive) properties involve the water retention function defining the relationship between the volumetric water content, θ , and the pressure head, h , and the hydraulic conductivity function defining the hydraulic conductivity, K , as a function of h or θ .

Water retention in soils is governed by capillarity at relatively high water contents, and adsorption at low water contents [*Jury and Horton*, 2004]. These two regions of the retention curve are often most noticeable for relatively coarse-textured (sandy) soils [*Sakai and Toride*, 2007; *Sakai et al.*, 2009; *Schelle et al.*, 2013]. Hysteresis in the hydraulic functions, furthermore, is important in especially the capillary region at relatively high water contents [*Huang et al.*, 2005; *Poulovassilis and Childs*, 1971; *Sakai et al.*, 2009]. Hysteresis may also exist in the adsorption region [*Arthur et al.*, 2015; *Davis et al.*, 2009; *Globus and Neusypina*, 2006; *Prunty and Bell*, 2007]. However, because hysteresis in the adsorb region occurs over only a small part of the retention function, its effect is probably negligible for many or most practical applications [*Sakai et al.*, 2009; *Schelle et al.*, 2013].

For the unsaturated hydraulic conductivity, one may similarly distinguish distinct capillary and film flow areas at relatively high and low water contents, respectively [*Lebeau and Konrad*, 2010; *Peters*, 2013; *Sakai and Toride*, 2007; *Zhang*, 2011]. Water in the very dry range can move furthermore in the form of vapor, while liquid flow may cease there [*Mehta et al.*, 1994; *Philip and De Vries*, 1957; *Saito et al.*, 2006]. Clearly,

comprehensive models for simulating water flow in field soils may require hydraulic functions that consider all of these different water retention and hydraulic conductivity properties and processes from saturation all the way to complete dryness.

Various hydraulic functions have been used over the years to describe capillary retention [Brooks and Corey, 1964; Kosugi, 1996; van Genuchten, 1980], while the capillary conductivity has been described using a range of statistical pore size distribution models such as those formulated by Burdine [1953] and Mualem [1976a]. The resulting classical capillary-based functions typically hold between saturation, θ_s , and some residual water content, θ_r . Many subsequently attempted to describe the capillary and adsorption regions for the complete water retention curve from saturation to complete dryness [Campbell and Shiozawa, 1992; Fayer and Simmons, 1995; Fredlund and Xing, 1994; Groenevelt and Grant, 2004; Khlosi et al., 2006; Lu et al., 2014; Rossi and Nimmo, 1994]. Most of these studies focused only on the water retention curve, while still neglecting the contribution of film conductivity to the overall hydraulic conductivity function. An early exception was a study by Fayer and Simmons [1995] in which the complete water retention functions were coupled with the capillary bundle model of Mualem [1976a] to estimate the unsaturated hydraulic conductivity for the entire range of water contents. Their approach assumes that the capillary-based model can be used also at low-pressure heads where water is mostly held in place by adsorptive rather than capillary forces. An application of their model to both a sandy and an aggregated soils was shown by Sakai and Toride [2007]. Subsequent key contributions to improved descriptions of the unsaturated hydraulic conductivity using the capillary conductivity model of Mualem [1976a] in combination with a film flow component are by Lebeau and Konrad [2010], Peters and Durner [2008], and Zhang [2011].

More recently, Peters [2013] introduced a set of empirical soil hydraulic models from full saturation to complete dryness. His models assumed a clear partitioning between capillary and adsorptive water retention, but also accounted for capillary and film conductivities. Although the models showed good agreement with measured data, a possible shortcoming for some applications is the fact that the complete functions are not continuously differentiable at the connection point between capillary and adsorptive water retention regions, leading to a discontinuity of the soil water capacity, $d\theta/dh$. To solve this problem, Iden and Durner [2014] modified Peters' model by including an empirical function for adsorptive water retention to produce a continuously differentiable soil water retention function. Following Iden and Durner [2014] and Peters [2014], we hereafter refer to this model as the Peters-Durner-Iden (PDI) model. While providing an important contribution, the PDI model at present does not account for capillary hysteretic water retention. Moreover, the PDI conductivity model cannot be estimated directly from water retention parameters [Peters, 2013] since it requires two extra parameters to account for the contribution of film conductivity, as compared to the commonly used closed-form hydraulic models (e.g., those by Durner [1994], Kosugi [1996], or van Genuchten [1980]).

Concurrently, various models have been proposed also to describe capillary hysteresis in the soil water retention curve. Kool and Parker [1987] modified the empirical hysteresis model of Scott et al. [1983] to a form consistent with the van Genuchten [1980] function. Because its relatively simple yet realistic form, the Kool and Parker [1987] hysteresis model has been widely implemented in numerical codes for water flow such as HYDRUS [Šimůnek et al., 2008], SWAP [Kroes et al., 2008], and UNSAT-H [Fayer, 2000]. One drawback of the hysteresis model of Kool and Parker [1987] is that the scanning loops are not closed and as such can lead to artificial "pumping effects" that can move scanning curves outside of the main wetting or drying branches [Kool and Parker, 1987]. To avoid unclosed scanning loops, the model of Parker and Lenhard [1987], denoted here as the PL model, forces closure on the scanning curves. Although the resulting model improved the description of scanning curves consistent with the retention equations of van Genuchten [1980], the model fails to adequately describe water retention at low water contents [Fayer and Simmons, 1995]. Moreover, the PL model uses a modified version of the capillary bundle model of Mualem [1976a] as a predictor for the unsaturated hydraulic conductivity function [Lenhard and Parker, 1987]. As shown by Tuller and Or [2001], Mualem's [1976a] model often fails to describe the hydraulic conductivity in the medium to dry range since it neglects film and corner flow.

In this study, we propose a model that incorporates four processes in the complete moisture range, capillary hysteretic and adsorptive water retention and capillary and film conductivity, by combining the PDI-based VG and PL models. We also include a vapor model for the conductivity in very dry range. The model was

compared with measured hysteretic water retention data of a dune sand. We further used the model to determine capillary and film conductivities of the same dune sand as measured using the evaporation method. In addition, we evaluated relationships between parameters for the film conductivity and the water retention parameters of the PDI-based VG model using several published data sets. The relationships were validated further by comparison with other water retention and conductivity data sets.

2. Theoretical Development

In this section, we provide a detailed description of the soil hydraulic model between saturation and complete dryness. First, we briefly review the Peters-Durner-Iden (PDI) model since it provides the kernel of our approach, and then include hysteresis in the formulation.

2.1. The Peters-Durner-Iden (PDI) Model

The PDI model for water retention according to *Iden and Durner* [2014] is given by

$$\begin{aligned}\theta(h) &= \theta^{cap}(h) + \theta^{ad}(h) \\ &= (\theta_s - \theta_r) S^{cap}(h) + \theta_r S^{ad}(h)\end{aligned}\quad (1)$$

where θ is the water content, h is the pressure head, $S^{cap}(h)$ is relative saturation of capillary water, and $S^{ad}(h)$ is relative saturation of adsorptive water. The residual water content, θ_r , hence serves as the maximum adsorptive water content. As shown by *Peters* [2013], $S^{cap}(h)$ can be parameterized by a unimodal pore size distribution function such as the *Kosugi* [1996] and *van Genuchten* [1980] equations, or a multimodal function [*Durner*, 1994]. To ensure that the water content becomes zero at some large value of the pressure head, h_0 (generally about -10^7 cm), *Iden and Durner* [2014] defined $S^{cap}(h)$ by rescaling the effective capillary function, $\Gamma(h)$, as follows

$$S^{cap}(h) = \frac{\Gamma(h) - \Gamma(h_0)}{1 - \Gamma(h_0)} \quad (2)$$

where $\Gamma(h)$ can be any of the standard functions [*Brooks and Corey*, 1964; *Kosugi*, 1996; *van Genuchten*, 1980]. For the function of *van Genuchten* [1980] as used further in this study, $\Gamma(h)$ is given by

$$\Gamma(h) = \left[\frac{1}{1 + (\alpha|h|)^n} \right]^m \quad (3)$$

In which α and n are essentially empirical shape parameters, and $m = 1 - 1/n$.

Iden and Durner [2014] introduced a smooth piecewise linear function to describe the relative saturation of adsorptive water:

$$S^{ad}(h) = 1 + \frac{1}{x_a - x_0} \left\{ x - x_a + b \ln \left[1 + \exp \left(\frac{x_a - x}{b} \right) \right] \right\} \quad (4)$$

where $x = \log_{10}(|h|)$, $x_0 = \log_{10}(|h_0|)$, $x_a = \log_{10}(|h_a|)$, and b is a smoothing parameter given by [*Iden and Durner*, 2014]

$$b = 0.1 + \frac{0.2}{n^2} \left\{ 1 - \exp \left[- \left(\frac{\theta_r}{\theta_s - \theta_r} \right)^2 \right] \right\} \quad (5)$$

Note that x in equation (4) is identical to the pF value as used in many soil water retention and plant water stress studies beginning with an early study by *Schofield* [1935]. We refer to *Iden and Durner* [2014] for a more detailed discussion of equations (4) and (5).

The hydraulic conductivity function for liquid flow is given by the sum of the capillary and film conductivities [*Peters*, 2013]:

$$\begin{aligned}K^{liq} &= K^{cap} + K^{film} \\ &= K_s^{cap} K_r^{cap} (S^{cap}) + K_s^{film} K_r^{film} (S^{ad})\end{aligned}\quad (6)$$

where the superscripts *liq*, *cap*, and *film* refer to liquid, capillary, and film contributions, respectively, K_s^{cap} and K_s^{film} are capillary and film conductivities at saturation, K_r refers to scaled or relative hydraulic

conductivities as a function of effective saturation of the capillary (S^{cap}) and film flow or adsorptive (S^{ad}) regions.

When the original *van Genuchten* [1980] soil hydraulic functions are used (i.e., equation (3) for the effective capillary function), the scaled hydraulic conductivity function is given by [Peters, 2014]

$$K_r^{cap} = (S^{cap})^\ell \left(1 - \left(\frac{1 - \Gamma(h)^{1/m}}{1 - \Gamma(h_0)^{1/m}} \right)^m \right)^2 \quad (7)$$

where ℓ is an empirical pore tortuosity and/or connectivity parameter that is generally assumed to be 0.5 [Mualem, 1976a]. The film conductivity as a function of S^{ad} is given by [Peters, 2013]:

$$K_r^{film} = \left(\frac{h_0}{h_a} \right)^{a(1-S^{ad})} \quad (8)$$

where h_a is an air entry value approximated by the value of $1/\alpha$ in van Genuchten's retention model, and a an empirical parameter [Peters, 2013].

Equation (6) reflects the contributions of both the capillary conductivity at relatively high water contents, as well as of the film conductivity at low water contents, to the overall liquid conductivity. In the very dry range, vapor transport may become more dominant than liquid flow [Mehta *et al.*, 1994, among others]. For vapor flow, one may assume that the gradient in the gravitational potential can be assumed negligible. This allows one to add the isothermal conductivity (K^{vh}) to the liquid conductivity to give the total conductivity (K^{tot}) as follows [e.g., Peters, 2013]:

$$K^{tot} = K^{liq} + K^{vh} = K^{cap} + K^{film} + K^{vh} \quad (9)$$

For completeness, details of the isothermal vapor conductivity, K^{vh} , are summarized in Appendix A, more or less following the development by Peters [2013]. We refer to the above PDI-based van Genuchten model as the PvG model. Next, we include in the formulation the effects of hysteresis involving both the main water retention branches (section 2.2) and the scanning curves (section 2.3).

2.2. Hysteresis Between the Main Retention Branches

We assumed that hysteresis occurs only in the capillary region of the water retention curve [Sakai *et al.*, 2009; Schelle *et al.*, 2013]. Thus, the hysteresis model of Parker and Lenhard [1987] is used here to describe the main drying and wetting curves of the capillary region, while equation (4) is used for adsorptive water retention without any hysteresis. The main drying and wetting curves for capillary retention in the PvG formulation are then described using:

$${}^d\Gamma(h) = \left[\frac{1}{1 + ({}^d\alpha|h|)^n} \right]^m \quad (10)$$

and

$${}^w\Gamma(h) = \frac{{}^w\theta_s - \theta_r}{{}^d\theta_s - \theta_r} \left[\frac{1}{1 + ({}^w\alpha|h|)^n} \right]^m \quad (11)$$

where $\Gamma(h)$ is the effective capillary function given earlier by equation (3), and where the prefatory superscripts d and w denote the main drying and wetting branches, respectively. When the main branches are closed at saturation, ${}^w\theta_s = {}^d\theta_s$, and hence ${}^d\Gamma(h) = {}^w\Gamma(h) = 1$ at $h = 0$. On the other hand, ${}^w\theta_s < {}^d\theta_s$ when the main branches are not closed at $h = 0$ due to entrapped air. Since ${}^d\Gamma(h)$ is assumed to be unity at $h = 0$, the effective capillary retention ${}^w\Gamma(h)$ for the wetting branch at $h = 0$ will be less than unity since the main wetting curve is scaled by the ratio $({}^w\theta_s - \theta_r)/({}^d\theta_s - \theta_r)$ as indicated by equation (11). And hence as a result, ${}^w\Gamma(h) \leq {}^d\Gamma(h) = 1$ for nonclosing main drying/wetting branches at $h = 0$.

Following Kool and Parker [1987], we assume that the hydraulic parameters of the main wetting and drying branches are identical, except for ${}^w\alpha < {}^d\alpha$. When the main branches are not closed at $h = 0$, an additional θ_s is needed since ${}^w\theta_s < {}^d\theta_s$, leading to a total of six parameters: θ_r , ${}^w\theta_s < {}^d\theta_s$, ${}^w\alpha < {}^d\alpha$, and n . The remaining

two water retention parameters associated with adsorptive water (h_a and h_0) were fixed. The value of h_a was set at $1/\alpha$ for both drying and wetting since adsorptive water retention is assumed to be nonhysteretic and often measured during drying, while h_0 was fixed at -6.3×10^6 cm as suggested by Peters [2013] based on Schneider and Goss [2011]. We note that the value of h_0 is very much consistent with recent measurements by Cobos *et al.* [2014] who showed that the zero water content intercepts of 13 well-characterized relatively coarse-textured soil occurred between 5.7 to 6.3 log kPa (or between -5×10^6 and -1.9×10^7 cm).

2.3. Scanning Curves

The scanning curve approach as used by Parker and Lenhard [1987] (PL) was used for capillary water retention. The PL model enforces closure of the scanning loops in terms of the effective water content, Γ . The reversal point in terms of effective water content, $(\Delta\Gamma, \Delta h)$, for reversal retention point $(\Delta\theta, \Delta h)$ is obtained by first subtracting $\theta^{ad}(\Delta h)$ from the reversal water content, $\Delta\theta$ (see equation (1)) to obtain the reversal point in terms of the capillary retention function, $(\Delta\theta^{cap}, \Delta h)$. Then, since ${}^w\theta_s < {}^d\theta_s$ and $0 \leq \Gamma \leq 1$, θ_s in equation (1) is equated to ${}^d\theta_s$ and $\Delta\Gamma$ is calculated using equations (1) and (2) to give

$$\Delta\Gamma = \frac{\Delta\theta^{cap}}{{}^d\theta_s - \theta_r} [1 - \Gamma(h_0)] + \Gamma(h_0) \approx \frac{\Delta\theta^{cap}}{{}^d\theta_s - \theta_r} \quad (12)$$

Consider a drying scanning curve which begins at the reversal point $(\Delta\Gamma_{wd}, \Delta h_{wd})$ from wetting to drying and proceeds to the drying end point at $(\Delta\Gamma_{dw}, \Delta h_{dw})$ before reversing from drying to wetting. The main drying curve is rescaled to interpolate between the reversal points using the following equation [Parker and Lenhard, 1987]:

$$\Gamma(h) = \frac{[\Delta\Gamma_{wd} - \Delta\Gamma_{dw}]}{[{}^d\Gamma(\Delta h_{wd}) - {}^d\Gamma(\Delta h_{dw})]} [{}^d\Gamma(h) - {}^d\Gamma(\Delta h_{dw})] + \Delta\Gamma_{dw} \quad (13)$$

where ${}^d\Gamma(\Delta h_{dw})$ and ${}^d\Gamma(\Delta h_{wd})$ are the values of ${}^d\Gamma(h)$ (equation (10)) at $h = \Delta h_{dw}$ and Δh_{wd} , respectively.

Consider similarly a wetting scanning curve starting at the reversal point $(\Delta\Gamma_{dw}, \Delta h_{dw})$, from drying to wetting to the wetting end point at $(\Delta\Gamma_{wd}, \Delta h_{wd})$, and then following the reversal from wetting to drying on the preceding drying curve. The main wetting curve is scaled to interpolate between the reversal points using [Parker and Lenhard, 1987]:

$$\Gamma(h) = \frac{[\Delta\Gamma_{dw} - \Delta\Gamma_{wd}]}{[{}^w\Gamma(\Delta h_{dw}) - {}^w\Gamma(\Delta h_{wd})]} [{}^w\Gamma(h) - {}^w\Gamma(\Delta h_{wd})] + \Delta\Gamma_{wd} \quad (14)$$

where ${}^w\Gamma(\Delta h_{dw})$ and ${}^w\Gamma(\Delta h_{wd})$ are values of ${}^w\Gamma(h)$ function given by equation (11) with $h = \Delta h_{dw}$ and Δh_{wd} , respectively.

If there is no entrapped air, then ${}^w\theta_s = {}^d\theta_s$ and hence ${}^d\Gamma_s = {}^w\Gamma_s = 1$. In contrast, if entrapped air exists, the main loop will not be closed at saturation since ${}^w\theta_s < {}^d\theta_s$ or ${}^w\Gamma_s < {}^d\Gamma_s$. Note that θ_u , which corresponds to Γ_u is defined by the water content at saturation as the end point of the primary scanning curve beginning from a reversal point at $(\Delta h_{dw}, \Delta\theta)$. Kool and Parker [1987] approximated Γ_u based on the Land formulation as discussed by Aziz and Settari [1979]:

$$\Gamma_u = 1 - \frac{1 - \Delta\Gamma_{dw}}{1 + R(1 - \Delta\Gamma_{dw})} \quad (15)$$

in which

$$R = \frac{1}{1 - {}^w\Gamma_s} - 1 \quad (16)$$

The primary wetting scanning curve is then calculated using equation (14) in which the end point of the primary wetting scanning curve at saturation is equal to $(\Delta\Gamma_{wd} = \Gamma_u, \Delta h_{wd} = 0)$ with a reversal point $(\Delta\Gamma_{dw}, \Delta h_{dw})$ on the main drying curve.

2.4. Hysteresis in the Hydraulic Conductivity

The hydraulic conductivity curve is calculated using equations (6)–(8). When the main branches are closed at $h = 0$, in which case ${}^w\theta_s = {}^d\theta_s = \theta_s$, the saturated hydraulic conductivity will be equal to

$dK_s^{cap} = {}^wK_s^{cap} = K_s^{cap}$ as given by equation (6). Equation (11) for ${}^w\Gamma(h)$ will then replace $\Gamma(h)$ in equation (7) for the wetting branch of the hydraulic conductivity, while equation (10) for $d\Gamma(h)$ is to replace $\Gamma(h)$ for the drying branch. However, when the main branches are not closed at $h = 0$, and hence ${}^w\theta_s < d\theta_s$ or ${}^w\Gamma_s < d\Gamma_s$, then dK_s^{cap} is used as the scale of the hydraulic conductivity, K_s^{cap} , in equation (6) for both drying and wetting. The approach is then in essence the same as the PvG model. The hydraulic conductivity curve of the proposed model contains four parameters: $K_s^{cap} = dK_s^{cap}$ and ℓ for the capillary conductivity and K_s^{film} and a for the film conductivity.

3. Soil Hydraulic Data Sets

Various data sets were used to test the PvG soil hydraulic model formulations. One set of experiments carried out using Tottori dune sand from Japan was to study the ability of the extended PvG model to describe hysteresis. We further used several published data sets from the literature to examine possible relationships between the water retention and film conductivity parameters.

The hysteretic water retention measurement of Tottori dune sand [Sakai and Toride, 2007] was carried out using the hanging water column method as applied to a soil sample 10 cm in diameter and 2.5 cm in height. Pressure heads and water contents of the soil were monitored using a tensiometer and a time domain reflectrometer (TDR) connected to a data logger. After saturation, drainage was initiated by decreasing the pressure head at the bottom of the column gradually until a pressure head of -60 cm. Rewetting was subsequently implemented using a Mariotte supply bottle by increasing the pressure head at the bottom of the column to saturation. The draining and wetting processes were repeated in the intermediate pressure head range to obtain various drying and wetting scanning curves. The observed hysteretic water retention data were obtained from the tensiometer and TDR readings. The pressure plate method was further used to measure water retention values between -500 and -1000 cm, while the vapor equilibrium method was used for water retention for pressure heads below -1000 cm. Both sets of measurements related to drying. The data were used to test the hysteresis description of the PvG formulation, and also the hydraulic conductivity between saturation and complete dryness.

In addition to the Tottori dune sand data, possible relationships between the two extra parameters in the film conductivity (i.e., K_s^{film} and a) and the PvG water retention parameters were evaluated using seven published data sets. The data sets comprised Sydney Sand [Minasny and Field, 2005]; Rhinluch Sand [Schindler and Müller, 2006]; Berlin Sand [Peters, 2013]; Gilat Loam, Rehovot Sand, and Pachapa Fine Sandy Clay [Mualem, 1976b]; and a Sandy Loam [Pachepsky et al., 1984]. All data sets pertained to the drying branches for both water retention and the hydraulic conductivity. Although half of the hydraulic conductivity data were situated between saturation and a pressure head of -1000 cm, the curves showed very distinct capillary and film conductivity components.

4. Results and Discussion

4.1. Hysteretic Capillary Retention

Figures 1a and 1b show the observed hysteretic water retention curves of Tottori dune sand on a logarithmic scale between pressure heads of -10^1 and -10^7 cm and on a linear scale between 0 and -60 cm, respectively. Water contents decreased rapidly between -20 and -50 cm, representing the capillary water retention region. Water contents subsequently decreased only slowly with decreasing pressure heads ($h < -50$ cm), typical of the adsorptive water retention region. The nonclosing nature of the main drying and wetting curves near saturation ($h = 0$) is clearly visible, indicating air entrapment during rewetting in the capillary region. Moreover, the main wetting and drying branches merged well in the dry region for $h < -50$ cm. This suggests that hysteresis may be negligible in the adsorptive water retention region of this sandy soil.

To test the hysteresis model, all data from the main drying and wetting curves in Figure 1a between 0 and -60 cm, as well as the data for $h < -100$ cm, were used to estimate the various model parameters in equations (1), (2), (4), (5), (10), and (11). This was done using a nonlinear least squares optimization approach that minimized the root-mean-square error (RMSE) between the calculated and observed data. We optimized six parameters (θ_r , ${}^w\theta_s$, $d\theta_s$, ${}^w\alpha$, $d\alpha$, and n), while the remaining three parameters were fixed: h_a at $1/d\alpha$ and h_0 at

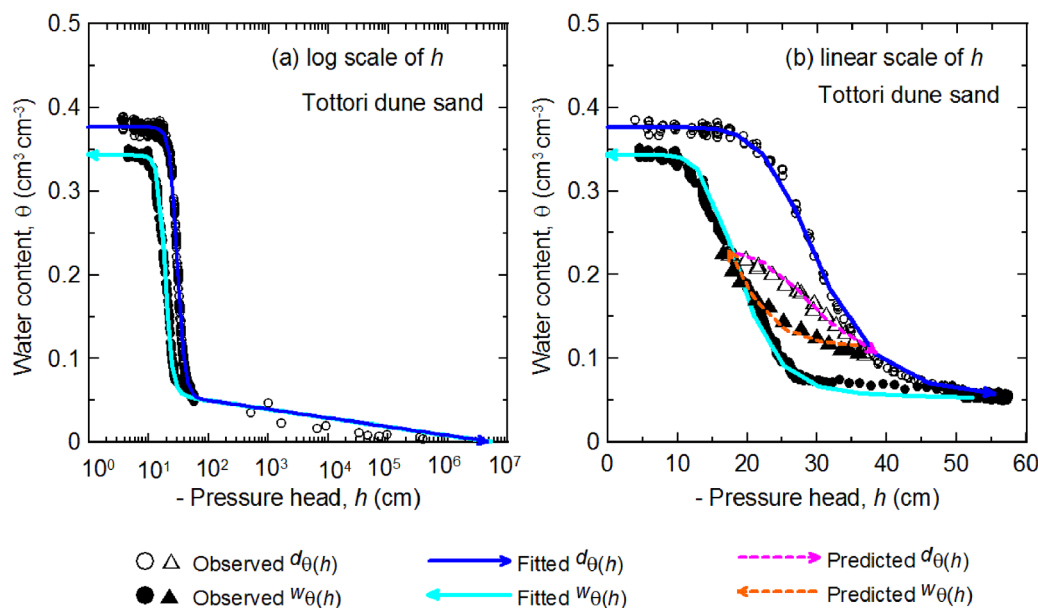


Figure 1. Observed capillary hysteretic and adsorptive water retention curves (open circle, triangle, solid circle, and solid triangle), their fitted main branches (solid lines) and predicted scanning curves (dash lines) for Tottori dune sand. Results are plotted versus in a (a) \log_{10} scale and (b) linear scale.

-6.3×10^6 cm as indicated earlier, and b as given by equation (5). The various parameter estimation calculations in this study were carried out using the Solver add-in of Microsoft Excel®.

Figures 1a and 1b show excellent agreement between the observed and fitted main branches using the optimized parameter values listed in Table 1. Drying and wetting processes are indicated by the direction of the arrows. The proposed PvG model could describe hysteretic capillary water retention very well for $h > -50$ cm, but also nonhysteretic retention in the adsorption region for $h < -50$ cm. Since the model accounts for air entrapment, the nonclosing main branches at and near saturation could be described equally well. Note from Table 1 that, as expected, the fitted θ_s and α parameters for the main drying and wetting curves differed (i.e., $d\alpha < w\alpha$ and $w\theta_s < d\theta_s$).

Figure 1b shows that the model could describe both scanning curves very well also, with the drying scanning curve initially moving from a reversal point on the main wetting branch ($h = -17.5$ cm, $\theta = 0.227$ cm³ cm⁻³) to some end point ($h = -36.5$ cm, $\theta = 0.115$ cm³ cm⁻³), followed by a wetting scanning curve back from the end point to the initial reversal point on main wetting curve. The model produced closed scanning curves as observed also in this experiment. We emphasize that the proposed model is relatively straightforward to apply since it requires only two additional parameters, $d\alpha$ and $d\theta_s$ (or $w\alpha$ and $w\theta_s$) to describe capillary hysteretic water retention as compared to the original PDI model.

4.2. Unsaturated Hydraulic Conductivity

Figure 2a shows the unsaturated hydraulic conductivity of Tottori dune sand as a function of the pressure head as estimated by Sakai and Toride [2007] using the evaporation method. Their parameter approach

Table 1. Soil Hydraulic Parameters for the Main Drying and Wetting Curves of the PDI-Based vG Model for Seven Soil Samples

	θ_r (cm ³ cm ⁻³)	$d\theta_s$ (cm ³ cm ⁻³)	$w\theta_s$ (cm ³ cm ⁻³)	$d\alpha$ (cm ⁻¹)	$w\alpha$ (cm ⁻¹)	n	K_s^{cap} (cm d ⁻¹)	ℓ	a	K_s^{film} (cm d ⁻¹)
Tottori Dune Sand	0.056	0.377	0.343	0.034	0.054	7.40	97.8	-0.11	-2.010	0.0480
Guelph Loam	0.286	0.519	0.434	0.013	0.036	2.59	31.6	0.5	-1.419	0.0068
Ida Silt Loam (0–15 cm)	0.166	0.542	0.494	0.009	0.015	1.47	491.0	0.5	-1.265	0.0015
Ida Silt Loam (>15 cm)	0.164	0.524	0.486	0.014	0.018	1.56	1082.9	0.5	-1.278	0.0039
Rubicon Sandy Loam	0.191	0.378	0.378	0.011	0.039	5.80	48.1	0.5	-1.866	0.0120
Rideau Clay Loam	0.304	0.419	0.419	0.018	0.054	3.63	20.0	0.5	-1.565	0.0098
Wray Dune Sand	0.106	0.303	0.303	0.030	0.053	8.20	514.0	0.5	-2.200	0.0140

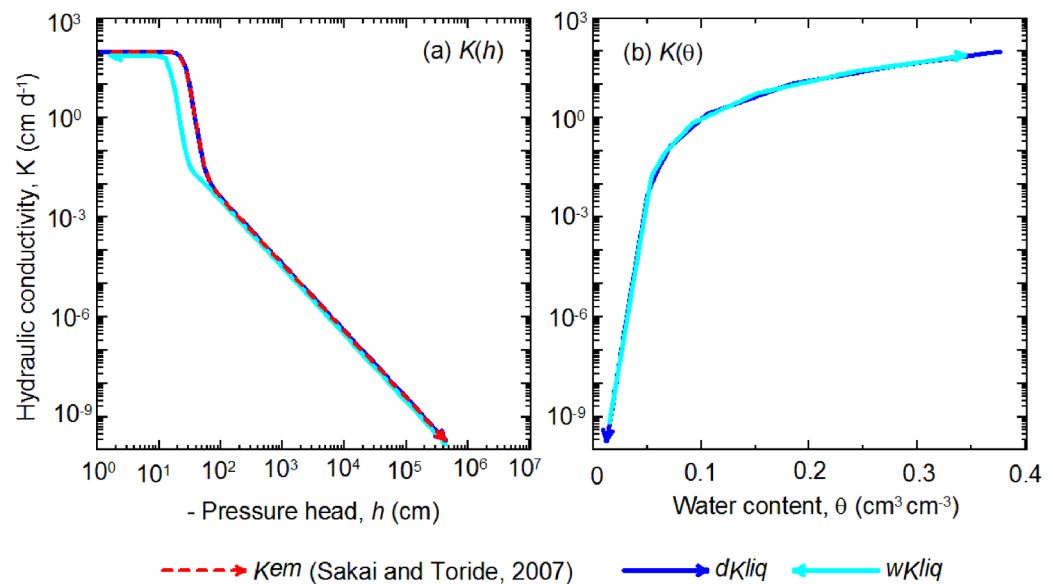


Figure 2. Liquid conductivities ($^dK^{liq}$ and $^wK^{liq}$) for the main drying and wetting branches of water retention of Tottori dune sand in Figure 1 (dark and light blue solid lines, respectively), and hydraulic conductivities (K^{em}) as estimated by Sakai and Toride [2007] using the evaporation method (orange dash lines). Results are plotted as a function of (a) pressure head and (b) water content.

assumed that the water retention and hydraulic conductivity curves could be described with the Fayer and Simmons [1995] and Mualem [1976a] models, respectively [Sakai and Toride, 2007]. The $K(h)$ curve in Figure 2a consists of two subcurves indicating the presence of capillary and film conductivities at relatively high and low-pressure heads, respectively. Figure 2a also shows the fitted $^dK(h)$ drying curve using water retention parameters of the main drying curve (Table 1). Since the PvG-based $K(h)$ model required four additional parameters (i.e., K_s^{cap} , ℓ , K_s^{film} , and a), those parameters were estimated by minimizing the RMSE between $\log_{10}K(h)$ model predictions and $\log_{10}K(h)$ observed data, while keeping the retention parameters fixed at the optimized values for the main drying curve as listed in Table 1. The various hydraulic parameters were used subsequently to predict the hydraulic conductivity $^wK(h)$ for the main wetting curve. Good agreement was obtained between $^dK(h)$ and $K(h)$ from the evaporation method. Capillary hysteresis caused the main $K(h)$ branches to be hysteretic also, as well as produced unclosed $K(h)$ curves at saturation. In accordance with the current model formulation, the film conductivity is assumed to be nonhysteretic.

The wetting and drying hydraulic conductivity curves as a function of water content, $K(\theta)$, are presented in Figure 2b. The curves appear almost nonhysteretic over the entire range of water contents, which is consistent with the often assumed nonhysteretic nature of $K(\theta)$ [Kool and Parker, 1987; Mualem, 1986; van Genuchten, 1980]. The main difference concerns the conductivity values of the unclosed main drying and wetting branches of their end points (at $h = 0$), leading to different values for $^d\theta_s$ and $^w\theta_s$.

4.3. Estimated Parameters of the Film Conductivity Model

One limitation of the PDI model is that it cannot be used to predict the film conductivity from the water retention parameters since two additional film conductivity parameters (K_s^{film} and a) are involved [Peters, 2013]. For this reason, we evaluated possible relationships between the water retention and film conductivity parameters of Tottori dune sand as well as of six other soil samples having a broad range of n values ($1.6 \leq n \leq 8$) and α values ($0.011 \leq \alpha \leq 0.054$) as described in Table 2.

The parameter estimation procedure was essentially the same as for the hysteretic data sets. First, we fitted the water retention parameters to the data using equations (1), (2), (3), and (4). Equations (6)–(8) were subsequently fitted to the hydraulic conductivity data, leading to estimates of the four conductivity parameters (i.e., K_s^{cap} and ℓ for the capillary conductivity, and K_s^{film} and a for the film conductivity), while keeping the retention parameters at their previously fitted values. Figure 3 shows a schematic of the capillary, film, and total conductivities, as well as of the locations of K_s^{cap} , K_s^{film} , h_{cf} , and $K^{cap}(h_{cf})$. We used h_{cf} for the pressure

Table 2. Soil Hydraulic Parameters of the PDI-Based vG Model for 11 Soil Samples

	θ_r (cm ³ cm ⁻³)	θ_s (cm ³ cm ⁻³)	A (cm ⁻¹)	n	K_s^{cap} (cm d ⁻¹)	ℓ	a	K_s^{film} (cm d ⁻¹)	h_{cf} (cm)	$K_c(h_{cf})$ (cm d ⁻¹)
Tottori Dune Sand	0.056	0.375	0.034	8.05	97.4	-0.147	-2.125	0.0795	-55.2	0.00576
Sydney Sand	0.041	0.427	0.027	7.30	58.7	-0.243	-1.796	0.0049	-95.4	0.00017
Rhinluch Sand	0.094	0.347	0.018	5.15	32.8	0.104	-2.435	0.0152	-137.4	0.00119
Berlin Sand	0.030	0.305	0.054	4.44	538.3	0.500	-1.722	0.0123	-66.2	0.00044
Gilat Loam	0.156	0.437	0.017	3.42	19.4	1.175	-1.238	0.0078	-164.8	0.00040
Revolholt Sand	0.020	0.402	0.045	3.22	2189.5	1.753	-1.433	0.0016	-114.5	0.00004
Pachappa Fine Sandy Clay	0.106	0.324	0.011	2.70	15.8	0.137	-1.561	0.0094	-492.0	0.00055
Sandy Loam	0.047	0.418	0.011	1.64	12.8	0.002	-1.165	0.0010	-3047.0	0.00002
Shonai Sand	0.058	0.419	0.041	8.05	673.0	0.5	-1.813	0.0641	-50.6	0.03468
Pachappa Loam	0.118	0.441	0.007	7.30	12.0	0.5	-1.416	0.0037	-759.6	0.00029
Adelanto Loam	0.237	0.426	0.004	5.15	5.0	0.5	-1.428	0.0024	-1275.7	0.00014

head at which $K^{cap}(h_{cf})$ is approximately equal to $K^{film}(h_{cf})$. Please note that in reality, K_s^{film} is always higher than $K^{cap}(h_{cf})$.

Results of the parameter analysis of the seven soils were used to correlate the film hydraulic parameters with the fitted retention parameters. Results of the analysis are shown graphically in Figure 4. The relationship between $\log_{10}(\alpha|h_{cf}|)$ and n is presented in Figure 4a. The plot suggested a hyperbolic type relationship, which we described using the completely empirical expression:

$$\log_{10}(\alpha|h_{cf}|) = 0.219 + 3.811n^{-2.187} \quad (17)$$

This function agreed reasonably well with the data, giving an R^2 value of 0.96.

Figure 4b shows a positive and relatively strong correlation (with $R^2 = 0.98$) between $\log_{10}[K^{cap}(h_{cf})]$ and $\log_{10}[K_s^{film}]$ using the function

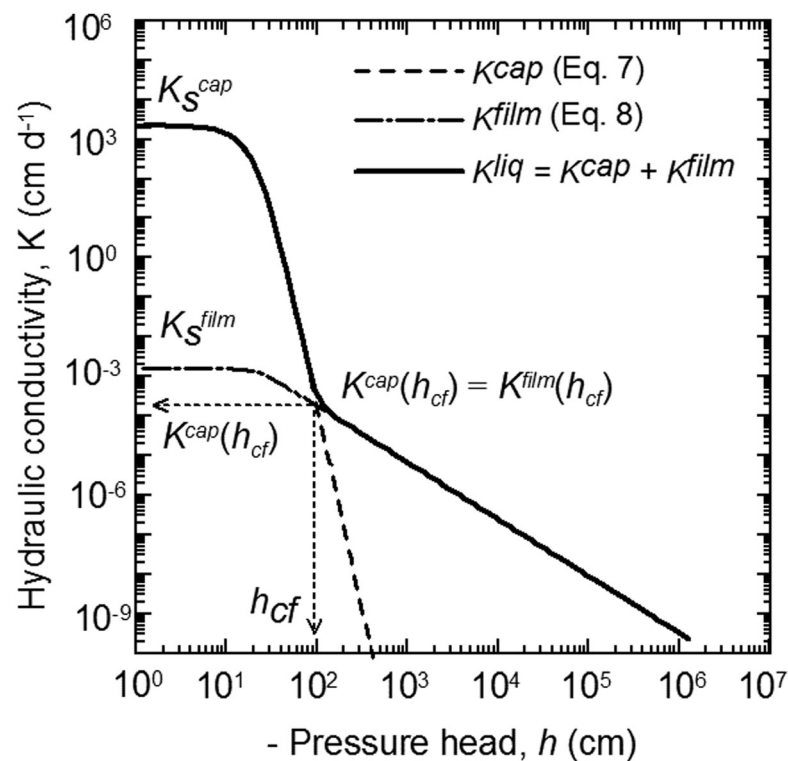


Figure 3. Schematic locations of K_s^{cap} , K_s^{film} , $K^{cap}(h_{cf})$, and h_{cf} on the capillary conductivity (black dash lines), film conductivity (black dash dot lines), and total conductivity curves (black solid lines).

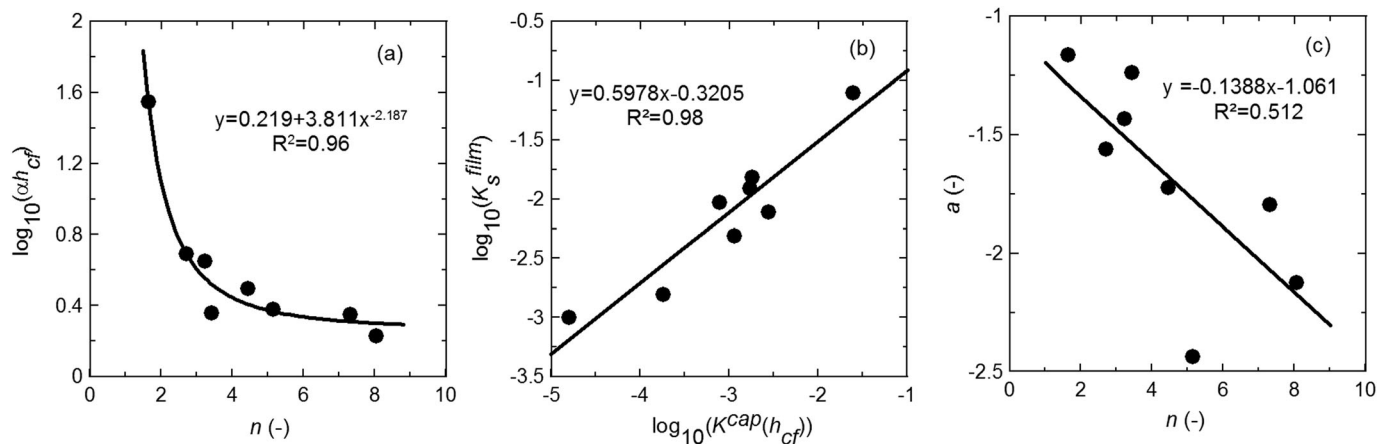


Figure 4. Relationships obtained for the water retention parameters n and α , and the film conductivity parameters K_s^{film} and a . The plots are for (a) n versus $\log_{10}(\alpha h_{cf})$; (b) $\log_{10}[K_s^{\text{film}}]$ versus $\log_{10}[K^{\text{cap}}(h_{cf})]$, and (c) n versus a .

$$\log_{10}[K_s^{\text{film}}] = 0.5978\{\log_{10}[K^{\text{cap}}(h_{cf})]\} - 0.3205 \quad (18)$$

Figure 4c shows the correlation between n and a , in this case, a negative correlation with $R^2 = 0.512$. The negative correlation suggests that a relatively steep capillary conductivity function, $K^{\text{cap}}(h)$, also will lead to a relatively steep film conductivity function, $K^{\text{film}}(h)$. This is to be expected since coarser soils, and soils having a relatively narrow pore or particle-size distribution, generally have higher values of n [e.g., *Carsel and Parrish*, 1988], leading to more rapidly declining film conductivities when they dry out. For the data in Figure 4c, we obtained a linear function between n and a :

$$a = -0.1388n - 1.061 \quad (19)$$

Equation (19) indicates that a in equation (8) may not be a constant as assumed by *Peters* [2013] in his model (he suggested a constant value of -1.5). According to the extended film conductivity model of *Tokunaga* [2009], specific surface area influences the slope of the film conductivity function. Since the specific surface area in turn is also related to the value of n (i.e., coarser soils generally have higher n values), some dependency of a on n is to be expected. Another possibility of why a is not constant in our study may be due to the assumption that h_a equals $1/\alpha$ in equation (8), which may have slightly affected the values of a during the parameter estimation analysis.

4.4. Validation of the Film Conductivity Parameters

We further tested the empirical relationships for the film flow parameters (equations (17)–(19)) by predicting the unsaturated hydraulic conductivity, $K(\theta)$ of three soils: Shonai Sand [*Mehta et al.*, 1994], Adelanto Loam, and Pachappa Loam [*Jackson et al.*, 1965; *Zhang*, 2011]. The complete water retention and hydraulic conductivity curves of those three soils were available from wet to dry as shown in Figure 5. After optimizing the water retention parameters of the PvG model (θ_r , θ_s , α , n), the two extra parameters (K_s^{film} and a) of the film conductivity model were determined. The parameter K_s^{film} was calculated using equation (18) assuming $\ell = 0.5$ for $K^{\text{cap}}(h_{cf})$ in equation (7), and with h_{cf} determined by equation (17). The parameter a was approximated using equation (19) as a function of n . The optimized retention parameters of the PvG model and the estimated parameters (K_s^{film} and a) in the film conductivity model for the three soils are listed in Table 2.

The corresponding fitted water retention and unsaturated hydraulic conductivity curves are shown in Figure 5. Results show that the PvG model agrees well the observed water retention of three soils from the wet to dry end. Furthermore, the model could predict the observed unsaturated hydraulic conductivity over the entire range of water contents excellently. This indicates that the capillary hydraulic conductivity model based on the van Genuchten-Mualem equations in combination with the film conductivity model of *Peters* [2013] and the empirical expressions given by equations (17)–(19) could describe the liquid conductivity quite well, including the film conductivity. Note that the n values in our study ranged from 1.6 to 8, and hence that the equations are valid only for this range.

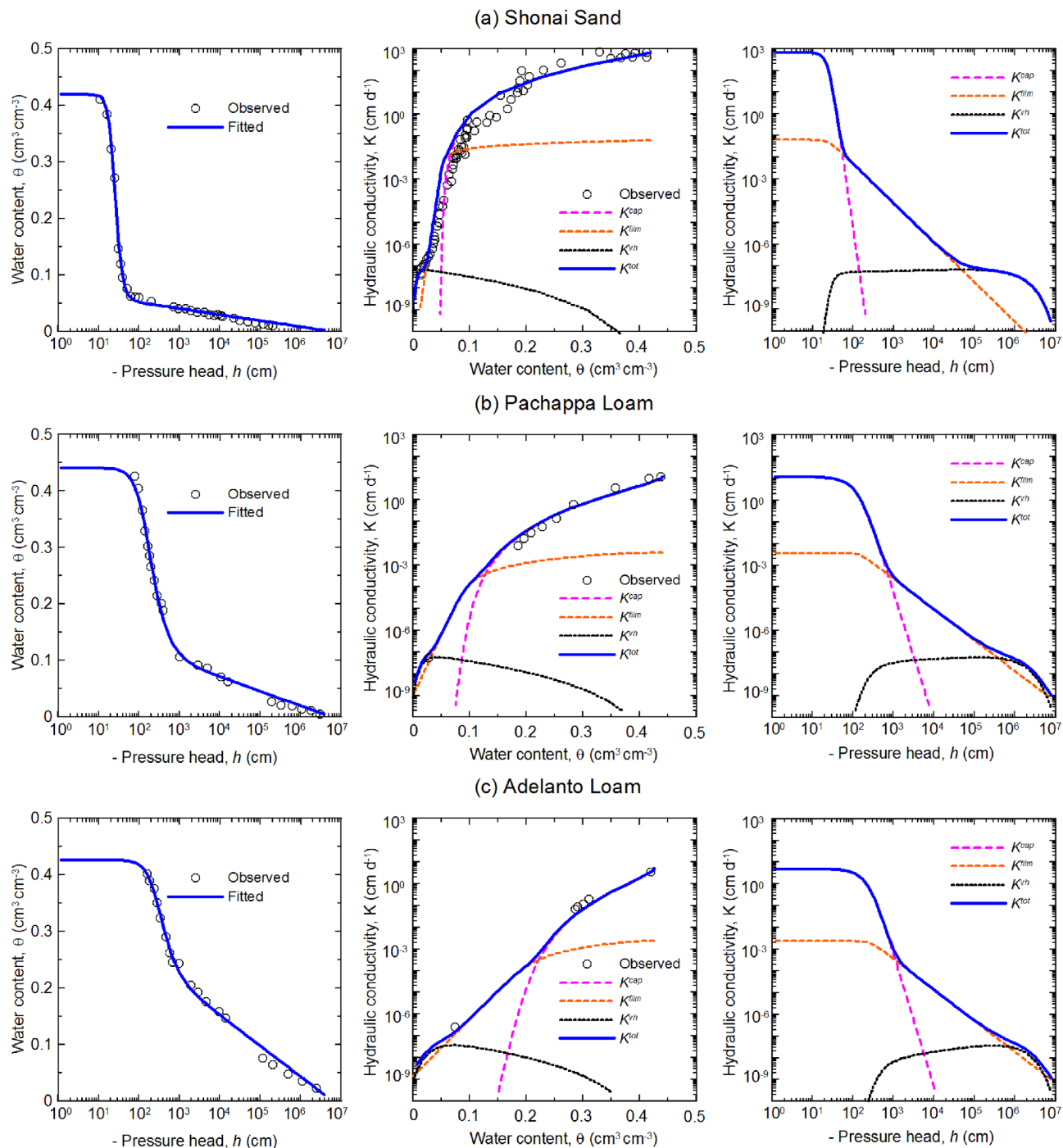


Figure 5. (left) Observed and fitted water retention, $\theta(h)$ and observed and predicted unsaturated hydraulic conductivity, $K(\theta)$ curves of (a) Shonai Sand, (b) Pachappa Loam, and (c) Adelanto Loam. Plotted are the capillary conductivity, K^{cap} (pink long dash lines), film conductivity, K^{film} (orange short dash lines), isothermal vapor conductivity, K^{vh} (light blue dot lines), and total conductivity, K^{tot} (dark blue solid lines) versus (middle) water content and (right) pressure head.

The plots in Figure 5 also show the contributions of the isothermal vapor conductivity, K^{vh} , to the total conductivity, K^{tot} . Calculations of K^{vh} using the approach summarized in Appendix A assumed that the temperature for vapor conductivity is equal to 20°C, which is a common laboratory condition [Peters, 2013]. Results show that the vapor conductivity curve, K^{vh} , becomes more dominant than the liquid conductivity when K^{liq} is less than about 5×10^{-8} cm d⁻¹, or for volumetric water contents less than about 0.025 for Shonai Sand (Figure 5a), 0.03 for Pachappa Loam (Figure 5b) and 0.05 cm³ cm⁻³ for Adelanto

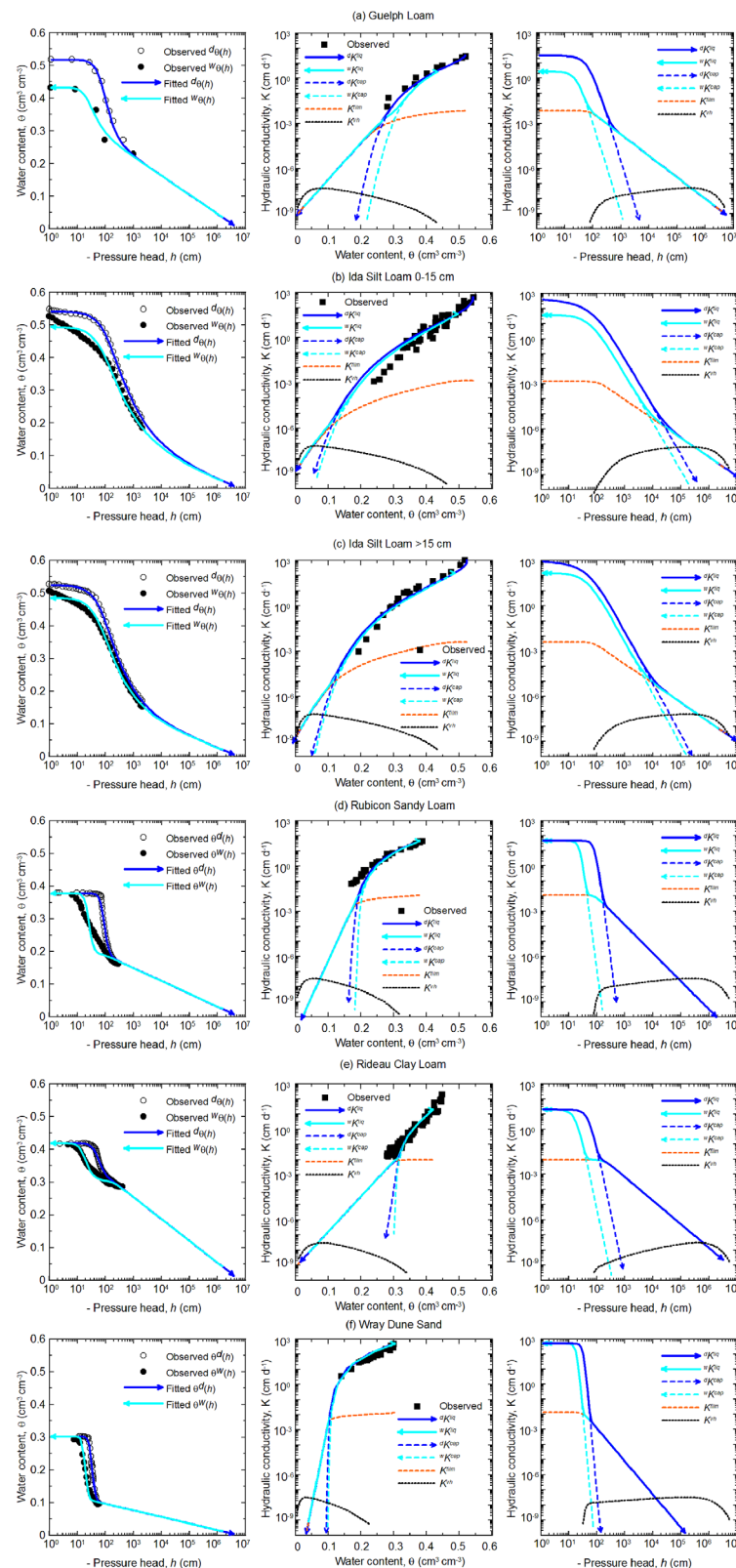


Figure 6. Application of the empirical equations for the film conductivity to estimate $K(\theta)$ in the whole water content range of (a) Guelph Loam, (b) Ida Silt Loam 0–15 cm, (c) Ida Silt Loam > 15 cm, (d) Rubicon Sandy Loam, (e) Rideau Clay Loam, and (f) Wray Dune Sand. Results are for the observed $\theta(h)$, $w_\theta(h)$, $K(\theta)$ data (symbols: open circle, solid circle, and solid square, respectively), the fitted $\theta(h)$ and $w_\theta(h)$ curves (dark and light blue solid lines), the predicted $\theta^{K^{cap}}$ and $w^{K^{cap}}$ curves (dark and light blue dash lines), and the predicted K^{cap} curves (black dotted lines). (left) $\theta(h)$, (middle) $K(\theta)$, and (right) $K(h)$.

Loam (Figure 5c). As demonstrated especially by the curves for Shonai Sand and Pachappa Loam, the contribution of the vapor conductivity to the total conductivity becomes more important than the film conductivity in the very dry range, ostensibly leading to an overall slightly better description of the conductivity data.

4.5. Further Tests of the Complete Soil Hydraulic Model Formulation

We conducted several additional tests to examine the complete hysteresis and conductivity features of the overall soil hydraulic model. We were especially interested in the utility of the derived empirical relationships, equations (17)–(19), for estimating the two extra parameters (K_s^{film} and a) of the film conductivity model. For the tests, we used unsaturated hydraulic conductivity data of eight soils ranging from clay loam to sand, including Guelph Loam [Erick and Bowman, 1964], Ida Silt Loam [Green et al., 1964], Rubicon Sandy Loam [Topp, 1969], Rideau Clay Loam [Topp, 1971], and Wray Dune Sand [Gillham et al., 1979]. Hysteretic water retention data of the eight soils were available only at relatively high-pressure heads as shown in Figure 6. The retention curves in the dry region were extrapolated to zero water contents at a value of -6.3×10^6 cm of the pressure head, h_0 , as suggested by Peters [2013] based on Schneider and Goss [2011].

To obtain the retention parameters, the observed main drying and wetting data were fitted simultaneously using the proposed hysteretic water retention model given by equations (1), (2), (4), (10), and (11). In total, six parameters were estimated (i.e., θ_r , $d\theta_s$, $w\theta_s$, $d\alpha$, $w\alpha$, and n), while the two remaining parameters were fixed ($h_a = 1/d\alpha$ and b). The $K(\theta)$ functions were predicted with K_s equated to the measured saturated hydraulic conductivities and assuming $\ell = 0.5$ [Mualem, 1976a]. The parameters h_{cf} , K_s^{film} , and a were furthermore estimated using equations (17)–(19), respectively.

The optimized parameters for the six soils are listed in Table 1 corresponding to the main drying and wetting branches and the calculated $K(\theta)$ curves in Figure 6. Although there are some disagreement for the main loop for Rubicon Sandy Loam and Rideau Clay Loam (Figures 6d and 6e), the hysteretic water retention model could describe both the drying and wetting retention curves very well. The predicted $K(\theta)$ curves (solid lines) for all eight soils were essentially nonhysteretic (i.e., $dK^{liq} \approx wK^{liq}$), and agreed well with the observed $K(\theta)$ values at the higher water content where the capillary conductivity dominates. Moreover, the liquid conductivity curves, K^{liq} at low water content were several orders of magnitudes higher than the capillary conductivity curves, K^{cap} , indicating that film conductivities, K^{film} contributed significantly to the overall liquid conductivity curves, K^{liq} .

The isothermal vapor conductivity K^{vh} components at 20°C for the eight soils are also shown in Figure 6. The isothermal vapor conductivity was found to clearly dominate the liquid conductivity in the dry end for the coarser soils with their relatively large n values (notably Wray Dune Sand and Rideau Clay Loam in Figures 6f and 6e, respectively). Conversely, the isothermal vapor conductivities of the more fine-textured soils (Ida Silt Loam 0–15 cm and > 15 cm in Figures 6a and 6b, respectively) with their smaller n values (broader pore size distributions) are very similar to the liquid conductivities in the dry end. Again, this phenomenon can be explained by the extended film conductivity model of Tokunaga [2009], which assumes that the film conductivity increases with increasing values of specific surface area. It follows that the film conductivities of finer-grained soils (with their smaller n values) are larger than those of coarser soils, which generally have larger n values and lower specific surface areas at similar porosities. As a result, the film conductivity of a finer-grained soil (with its larger specific surface area) will inch toward the values of isothermal vapor conductivity encountered at low-pressure heads.

5. Conclusions

We improved the PDI model by incorporating the Parker and Lenhard (PL) hysteresis model for capillary water retention in their formulation. The resulting combined model only requires two extra parameters as compared to the PDI model. The model includes capillary hysteresis at high water contents with either closed or unclosed main branches at full saturation due to entrapped air, closed scanning curves, and nonhysteretic adsorptive water retention at low water contents. The model could fit the main drying and wetting branches and predict the drying and wetting scanning curves of water retention very well.

The shape of the unsaturated hydraulic conductivity curve as a function of pressure head, $K(h)$, reflects the shape of water retention, with hysteresis present in the capillary conductivity but not in the film conductivity. The model yielded mostly nonhysteretic unsaturated hydraulic conductivity functions versus water content, $K(\theta)$, for the entire range of water contents. Inclusion of a vapor conductivity component in the model improved predictions in the very dry range. In this paper, we concentrated on descriptions of the water retention and unsaturated hydraulic conductivity curves. It would be interesting to implement the proposed model in numerical software for predicting various variably saturated flow processes, especially for relatively dry soil conditions (including evaporation and root water uptake processes). We believe that the model will increase the accuracy of predictions substantially since the approach accounts for many of the physical processes governing soil water retention and flow from saturation until complete dryness.

Water retention parameters could be related to the film conductivity parameters by establishing empirical models. The resulting combination of PvG and empirical relationships was validated using published data sets, with results showing that the proposed model is in close agreement with the data. Thus, with this model, the unsaturated hydraulic conductivity for whole range of water content can be readily calculated. Still, if both complete water retention and hydraulic conductivity data sets are available, it remains of course preferred to fit the adsorptive retention and film water retention and hydraulic parameters directly to the data.

Appendix A: Predicting Isothermal Vapor Hydraulic Conductivity

The isothermal vapor hydraulic conductivity, K^{vh} (m s^{-1}), is defined as [Mehta et al., 1994; Peters, 2013; Philip and De Vries, 1957; Saito et al., 2006; Sakai et al., 2009]:

$$K^{vh} = \frac{\rho_{vs}}{\rho_w} D \frac{Mg}{RT} H_r \quad (\text{A1})$$

where ρ_{vs} (kg m^{-3}) is the saturated vapor density, ρ_w ($= 1000 \text{ kg m}^{-3}$) is the density of liquid water, D ($\text{m}^2 \text{ s}^{-2}$) is the vapor diffusivity in soil, M is the molecular weight of water ($0.018015 \text{ kg mol}^{-1}$), g is the gravitational acceleration (9.81 m s^{-2}), R is the universal gas constant ($= 8.314 \text{ J mol}^{-1} \text{ K}^{-1}$), T (K) is the absolute temperature, and H_r is relative humidity. The vapor diffusivity, D , in soils can be derived as a product of the diffusivity of water vapor in air, D_a ($\text{m}^2 \text{ s}^{-2}$), the tortuosity factor in the gaseous phase, τ_a , and the volumetric air content, θ_a , using

$$D = \tau_a \theta_a D_a \quad (\text{A2})$$

The tortuosity factor in the gaseous phase, τ_a , may be calculated with the [Millington and Quirk, 1961] relationship:

$$\tau_a = \frac{\theta_a^{7/3}}{\phi^2} \quad (\text{A3})$$

where ϕ [–] is the porosity, assumed to be equal to θ_s for simplicity, and $\theta_a = \theta_s - \theta(h)$. The parameters D_a and ρ_{vs} are functions of temperature:

$$D_a = 2.14 \cdot 10^{-5} \left(\frac{T}{273.15} \right)^2 \quad (\text{A4})$$

and

$$\rho_{vs} = 10^{-3} \exp \left(31.3716 - \frac{6014.79}{T} - 7.92495 \cdot 10^{-3} T \right) T^{-1} \quad (\text{A5})$$

whereas H_r is derived using the Kelvin equation:

$$H_r = \exp \left(- \frac{Mg|h|}{RT} \right) \quad (\text{A6})$$

where h (m) is the pressure head.

Acknowledgments

We would like to thank A. Peters of the Institut für Ökologie, Technische Universität Berlin, Germany, for sharing some of the data sets used in this paper. The published data sets for this paper are properly cited and referred to in the reference list: Sydney Sand [Minasny and Field, 2005]; Rhinluch Sand [Schindler and Müller, 2006]; Berlin Sand [Peters, 2013]; Gilat Loam, Rehovot Sand, and Pachapa Fine Sandy Clay [Mualem, 1976b]; Sandy Loam [Pachepsky et al., 1984]; Shonai Sand [Mehta et al., 1994]; Adelanto Loam, and Pachappa Loam [Jackson et al., 1965; Zhang, 2011]; Guelph Loam [Erick and Bowman, 1964]; Ida Silt Loam [Green et al., 1964]; Rubicon Sandy Loam [Topp, 1969]; Rideau Clay Loam [Topp, 1971], and Wray Dune Sand [Gillham et al., 1979].

References

- Arthur, E., M. Tuller, P. Moldrup, D. K. Jensen, and L. W. De Jonge (2015), Prediction of clay content from water vapour sorption isotherms considering hysteresis and soil organic matter content, *Eur. J. Soil Sci.*, 66(1), 206–217, doi:10.1111/ejss.12191.
- Aziz, K., and A. Settari (1979), *Petroleum Reservoir Simulation*, Appl. Sci. Publ., London, U. K.
- Brooks, R. H., and A. T. Corey (1964), Hydraulic properties of porous media, *Hydrol. Pap.* 3, pp. 1–27, Colo. State Univ., Fort Collins, Colo.
- Burdine, N. T. (1953), Relative permeability calculations from pore size distribution data, *Trans. Am. Inst. Min. Metall. Pet. Eng.*, 198, 71–78.
- Campbell, G. S., and S. Shiozawa (1992), Prediction of hydraulic properties of soils using particle-size distribution and bulk density data, in *Proceedings of International Workshop, Indirect Methods for Estimating the Hydraulic Properties of Unsaturated Soils*, edited by M. Th. van Genuchten, F. J. Leij, and L. J. Lund, pp. 317–328, Univ. of Calif., Riverside, Calif.
- Carsel, R. F., and R. S. Parrish (1988), Developing joint probability distributions of soil water retention characteristics, *Water Resour. Res.*, 24, 755–769.
- Cobos, D. R., L. D. Rivera, and G. S. Campbell (2014), Can the dry-end (~1 to ~1000 MPa) soil water characteristic curve be well characterized with a single point?, paper presented at SSSA International Annual Meetings, Soil Science Society of America, Long Beach, Calif. [Available at <https://scisoc.confex.com/scisoc/2014am/webprogram/Paper87750.html>.]
- Collis-George, N. (2012), A re-interpretation of the drainage moisture characteristic, *Geoderma*, 189–190, 87–90, doi:10.1016/j.geoderma.2012.05.008.
- Davis, D. D., R. Horton, J. L. Heitman, and T. Ren (2009), Wettability and hysteresis effects on water sorption in relatively dry soil, *Soil Sci. Soc. Am. J.*, 73(6), 1947–1951, doi:10.2136/sssaj2009.00028N.
- Durner, W. (1994), Hydraulic conductivity estimation for soils with heterogeneous pore structure, *Water Resour. Res.*, 30, 211–223, doi:10.1029/93WR02676.
- Durner, W., and H. Flüher (2005), Soil hydraulic properties, in *Encyclopedia of Hydrological Sciences*, John Wiley, Hoboken, N. J.
- Erick, D. E., and D. H. Bowman (1964), Note on an improved apparatus for soil moisture flow measurements, *Soil Sci. Soc. Am. Proc.*, 28, 450–453.
- Fayer, M. J. (2000), *UNSAT-H Version 3.0: Unsaturated Soil Water and Heat Flow Model: Theory, User Manual, and Examples*, Pac. Northwest Natl. Lab., Richland, Wash.
- Fayer, M. J., and C. S. Simmons (1995), Modified soil water retention functions for all matric suctions, *Water Resour. Res.*, 31, 1233–1238.
- Fredlund, D. G., and A. Q. Xing (1994), Equations for the soil-water characteristic curve, *Can. Geotech. J.*, 31(4), 521–532.
- Gillham, R. W., A. Klute, and D. F. Heermann (1979), Measurement and numerical simulation of hysteretic flow in a heterogeneous porous medium, *Soil Sci. Soc. Am. J.*, 43, 1061–1067.
- Globus, A. M., and T. A. Neuspina (2006), Determination of the water hysteresis and specific surface of soils by electronic microhygrometry and psychrometry, *Eurasian Soil Sci.*, 39(3), 270–277, doi:10.1134/S1064229306030057.
- Green, R. E., R. J. Hanks, and W. E. Larson (1964), Estimates of field infiltration by numerical solution of the moisture flow equation, *Soil Sci. Soc. Am. J.*, 28, 15–19.
- Groenevelt, P. H., and C. D. Grant (2004), A new model for the soil water retention curve that solves the problem of residual water contents, *Eur. J. Soil Sci.*, 55, 479–485.
- Huang, H. C., Y. C. Tan, C. W. Liu, and C. H. Chen (2005), A novel hysteresis model in unsaturated soil, *Hydrol. Processes*, 19, 1653–1665.
- Iden, S. C., and W. Durner (2014), Comment on “Simple consistent models for water retention and hydraulic conductivity in the complete moisture range” by A. Peters, *Water Resour. Res.*, 50, 7530–7534, doi:10.1002/2014WR015937.
- Jackson, R. D., R. J. Reginato, and C. H. M. Van Bavel (1965), Comparison of measured and calculated hydraulic conductivities of unsaturated soils, *Water Resour. Res.*, 1, 375–380, doi:10.1029/WR001i003p00375.
- Jury, W., and R. Horton (2004), *Soil Physics*, 6th ed., 390 pp., John Wiley, N. Y.
- Khlosi, M., W. M. Cornelis, D. Gabriels, and G. Sin (2006), Simple modification to describe the soil water retention curve between saturation and oven dryness, *Water Resour. Res.*, 42, W11501, doi:10.1029/2005WR004699.
- Kool, J. B., and J. C. Parker (1987), Development and evaluation of closed-form expressions for hysteretic soil hydraulic properties, *Water Resour. Res.*, 23, 105–114, doi:10.1029/WR023i001p00105.
- Kosugi, K. (1996), Lognormal distribution model for unsaturated soil hydraulic properties, *Water Resour. Res.*, 32, 2697–2703, doi:10.1029/96WR01776.
- Kroes, J. G., J. C. van Dam, P. Groenendijk, R. F. A. Hendriks, and C. M. J. Jacobs (2008), *SWAP Version 3.2. Theory, Description and User Manual*, Alterra, Wageningen, Netherlands.
- Lebeau, M., and J.-M. Konrad (2010), A new capillary and thin film flow model for predicting the hydraulic conductivity of unsaturated porous media, *Water Resour. Res.*, 46, W12554, doi:10.1029/2010WR009092.
- Lenhard, R. J., and J. C. Parker (1987), A model for hysteretic constitutive relations governing multiphase flow: 2. Permeability-saturation relations, *Water Resour. Res.*, 23, 2197–2206, doi:10.1029/WR023i012p02197.
- Lu, S., T. Ren, Y. Lu, P. Meng, and S. Sun (2014), Extrapolative capability of two models that estimating soil water retention curve between saturation and oven dryness, *PLoS One*, 9(12), e113518, doi:10.1371/journal.pone.0113518.
- Mehta, B. K., S. Shiozawa, and M. Nakano (1994), Hydraulic properties of a sandy soil at low water contents, *Soil Sci.*, 157(4), 208–214.
- Millington, R., and J. P. Quirk (1961), Permeability of porous Solids, *Trans. Faraday Soc.*, 57(8), 1200–1207.
- Minasny, B., and D. J. Field (2005), Estimating soil hydraulic properties and their uncertainty: The use of stochastic simulation in the inverse modelling of the evaporation method, *Geoderma*, 126(3–4), 277–290, doi:10.1016/j.geoderma.2004.09.015.
- Mualem, Y. (1976a), A new model for predicting the hydraulic conductivity of unsaturated porous media, *Water Resour. Res.*, 12, 513–522, doi:10.1029/WR012i003p00513.
- Mualem, Y. (1976b), *A catalogue of the hydraulic properties of unsaturated soils, technical report*, Project Report No. 442, Tec.—Isr. Inst. of Technol., Haifa, Israel.
- Mualem, Y. (1986), Hydraulic conductivity of unsaturated soils: Prediction and formulas, in *Methods in Soil Analysis. Part 1, Agron. Monogr.*, vol. 9, 2nd ed., edited by A. Klute, pp. 799–824, Am. Soc. of Agron., Madison, Wis.
- Pachepsky, Y., R. Scherbakov, G. Varallyay, and K. Rajkai (1984), On obtaining soil hydraulic conductivity curves from water retention curves [in Russian], *Pochvovedenie*, 10, 60–72.
- Parker, J. C., and R. J. Lenhard (1987), A model for hysteretic constitutive relations governing multiphase flow: 1. Saturation-pressure relations, *Water Resour. Res.*, 23, 2187–2196, doi:10.1029/WR023i012p02187.
- Peters, A. (2013), Simple consistent models for water retention and hydraulic conductivity in the complete moisture range, *Water Resour. Res.*, 49, 6765–6780, doi:10.1002/wrcr.20548.

- Peters, A. (2014), Reply to comment by S. Iden and W. Durner on "Simple consistent models for water retention and hydraulic conductivity in the complete moisture range", *Water Resour. Res.*, *50*, 7535–7539, doi:10.1002/2014WR016107.
- Peters, A., and W. Durner (2008), A simple model for describing hydraulic conductivity in unsaturated porous media accounting for film and capillary flow, *Water Resour. Res.*, *44*, W11417, doi:10.1029/2008WR007136.
- Philip, J. R., and D. A. De Vries (1957), Moisture movement in porous materials under temperature gradients, *Trans. AGU*, *38*(2), 222–232, doi:10.1029/TR038i002p00222.
- Poulovassilis, A., and E. C. Childs (1971), The hysteresis of pore water: The non-independence of domains, *Soil Sci.*, *112*(5), 301–312.
- Prunty, L., and J. Bell (2007), Soil water hysteresis at low potential, *Pedosphere*, *17*(4), 436–444, doi:10.1016/S1002-0160(07)60053-8.
- Rossi, C., and J. R. Nimmo (1994), Modeling of soil water retention from saturation to oven dryness, *Water Resour. Res.*, *30*, 701–708, doi:10.1029/93WR03238.
- Saito, H., J. Šimůnek, and B. P. Mohanty (2006), Numerical analysis of coupled water, vapor, and heat transport in the vadose zone, *Vadose Zone J.*, *5*(2), 784–800, doi:10.2136/vzj2006.0007.
- Sakai, M., and N. Toride (2007), Soil water hydraulic functions for a sandy soil and an aggregated soil [in Japanese with English abstract], *J. Jpn. Soc. Soil Phys.*, *107*, 63–77.
- Sakai, M., N. Toride, and J. Šimůnek (2009), Water and vapor movement with condensation and evaporation in a sandy column, *Soil Sci. Soc. Am. J.*, *73*(3), 707–717, doi:10.2136/sssaj2008.0094.
- Schelle, H., L. Heise, K. Jänicke, and W. Durner (2013), Water retention characteristics of soils over the whole moisture range: A comparison of laboratory methods, *Eur. J. Soil Sci.*, *64*(6), 814–821, doi:10.1111/ejss.12108.
- Schindler, U., and L. Müller (2006), Simplifying the evaporation method for quantifying soil hydraulic properties, *J. Plant Nutr. Soil Sci.*, *169*(5), 623–629, doi:10.1002/jpln.200521895.
- Schneider, M., and K. U. Goss (2011), Temperature dependence of the water retention curve for dry soils, *Water Resour. Res.*, *47*, W03506, doi:10.1029/2010WR009687.
- Schofield, R. K. (1935), *The pF of the water in soil, paper presented at Transaction of 3rd International Congress of Soil Science*, International Union of Soil Sciences (IUSS), Oxford, U. K.
- Scott, P. S., G. J. Farquhar, and N. Kouwen (1983), *Hysteresis Effects on Net Infiltration*, *Advances in Infiltration*, pp. 163–170, Am. Soc. Agric. Eng., St. Joseph, Mich.
- Šimůnek, J. (2005), *Models of water flow and solute transport in the unsaturated zone*, in *Encyclopedia of Hydrological Sciences*, edited by M. G. A. J. J. McDonnell, chap. 78, pp. 1171–1180, John Wiley, Chichester, U. K.
- Šimůnek, J., M. Šejna, H. Saito, M. Sakai, and M. T. van Genuchten (2008), *The Hydrus-1D Software Package for Simulating the Movement of Water, Heat, And Multiple Solutes In Variably Saturated Media, Version 4.0*, *HYDRUS Software Ser. 3*, Dep. of Environ. Sci., Univ. of Calif., Riverside, Calif.
- Tokunaga, T. K. (2009), Hydraulic properties of adsorbed water films in unsaturated porous media, *Water Resour. Res.*, *45*, W06415, doi:10.1029/2009WR007734.
- Topp, G. C. (1969), Soil-water hysteresis measured in a sandy loam and compared with the hysteretic domain model, *Soil Sci. Soc. Am. J.*, *33*(5), 645–651, doi:10.2136/sssaj1969.03615995003300050011x.
- Topp, G. C. (1971), Soil water hysteresis in silt loam and clay loam soils, *Water Resour. Res.*, *7*, 914–920, doi:10.1029/WR007i004p00914.
- Tuller, M., and D. Or (2001), Hydraulic conductivity of variably saturated porous media: Film and corner flow in angular pore space, *Water Resour. Res.*, *37*, 1257–1276, doi:10.1029/2000WR900328.
- van Genuchten, M. T. (1980), A closed-form equation for predicting the hydraulic conductivity of unsaturated soils, *Soil Sci. Soc. Am. J.*, *44*(5), 892–898, doi:10.2136/sssaj1980.03615995004400050002x.
- Zhang, Z. F. (2011), Soil water retention and relative permeability for conditions from oven-dry to full saturation, *Vadose Zone J.*, *10*(4), 1299–1308, doi:10.2136/vzj2011.0019.